An Ideal Observer Approach to Beamforming

Craig K. Abbey,[1,2] Nghia Nguyen[3], and Michael F. Insana[3]

[1] Department of Psychology, University of California, Santa Barbara. USA.
[2] Department of Biomedical Engineering, University of California, Davis. USA.
[3] Departments of Bioengineering and ECE, and Beckman Institute for Advanced Science and Technology, University of Illinois at Urbana-Champaign. USA.

ABSTRACT

Many signal processing issues in ultrasonic imaging can be viewed as attempts to focus signal energy while preserving the diagnostic information they contain. We have been developing a task-based ideal-observer approach to signal processing with the goal of better understanding the factors that influence the transfer of diagnostic information and improving signal processing algorithms for optimal transfer. We treat the scattering medium as a Gaussian random field with non-uniform variance that encodes the properties necessary for accurate task performance. Using measured point-spread functions for a given system we propagate the scattering statistics through to various stages of the acquisition process along with acquisition noise. In this work we focus on the role of beamforming in this process. We consider the efficiency of information transfer by analyzing the ideal observer acting on individual receive elements and then considering different strategies for preserving diagnostic information in beamformed echo signals. Optimal beamforming strategies suggested by the analysis are approximated by applying spatial filtering techniques to fixed-focus echo data. These results are compared with a standard delay-and-sum beamformer.

Keywords: Beamforming, Breast Imaging, Ideal Observer.

1. INTRODUCTION

Beamforming is a critical component in the formation of backscattered ultrasound images whereby responses from an array of sensors are combined into a single radio-frequency (RF) signal[1,2]. It is challenging on a practical level because the process occurs in real time at video-rate speeds. However the process is also a theoretical challenge because it is not clear how the many received signals should be combined to optimally preserve the diagnostic information in them. The latter problem, finding optimal transforms for beamforming is the subject of this work.

In previous publications[3,4] we have developed a relatively simple statistical model of ultrasonic image formation that is based on a Gaussian stochastic process to represent the acoustic scattering of the object. A linear transformation of the object that is based on the pressure profile of the pulse models pulse-echo image formation. We restrict attention to the focal region of the pulse, which allows us to implement the linear system through convolution with a pulse point-spread function (PSF). This model of RF acquisition is combined with a panel of simple visual tasks related to breast cancer detection and diagnosis to evaluate and optimize signal processing. We approach this optimization by considering an optimal discriminant function, the (log) likelihood ratio, from signal detection theory[5]. In imaging tasks, this optimal discriminant is referred to as the ideal observer since it performs the visual task and achieves the best possible performance by a number of reasonable metrics[6,7].

In this work, we generalize our model of image formation to incorporate the formation of individual receive element signals. This allows us to consider the role of beamforming on task performance, and allows us to analyze the ideal observer for processing strategies that achieve optimal performance. For validation of the theory, we consider performance in five simple visual tasks related to breast cancer imaging using a system model based on Field II simulation code for acoustic pulse propagation in a scattering medium[8,9]. An analysis of the ideal observer decision variable suggests a matched filter tuned to the phase spectrum of the individual receive element pulse profiles. We have compared this approach to beamforming to standard delay-and-sum beamforming, and we find considerable improvement in 4 of the 5 tasks.

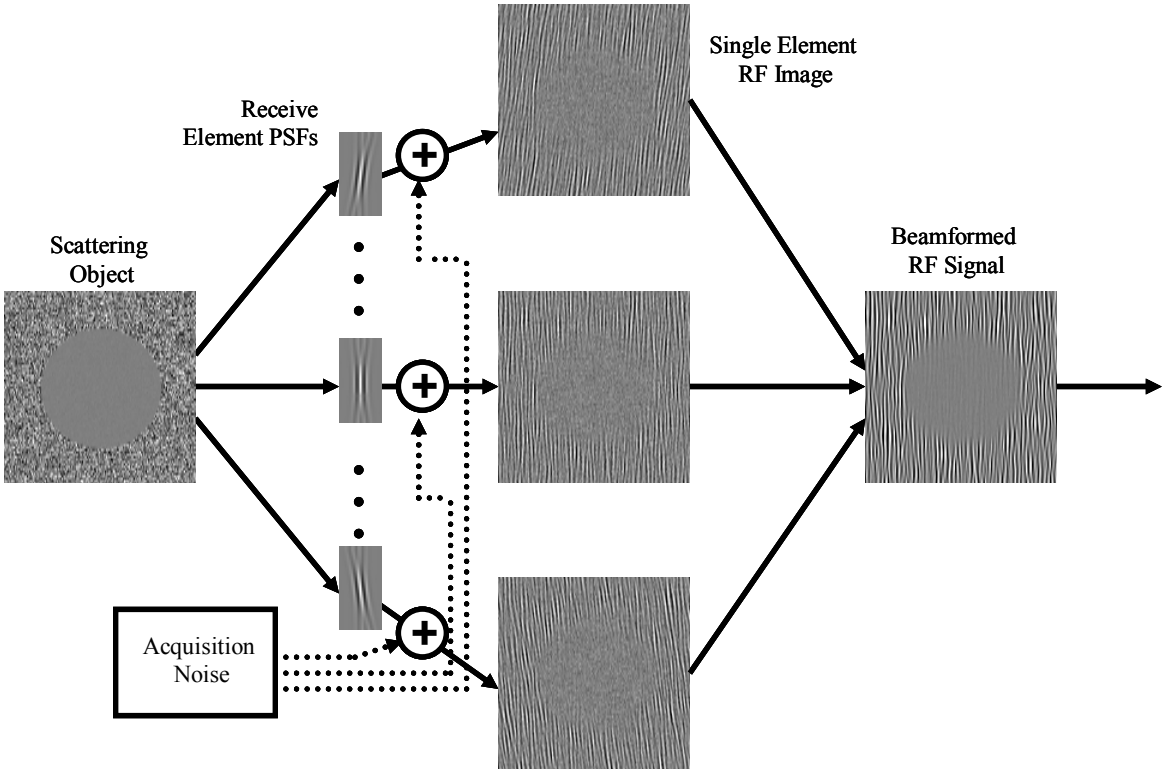

Figure 1. Model of acquisition and beamforming. This schematic diagram shows how a scattering object is transformed by a pulse profile and acquisition noise to form single receive element RF images (shown here scan converted into individual images). These are then combined across receive elements to make the beamformed RF signal.

2. THEORY

Figure 1 is a graphical diagram of the beamforming process as used in this work. An array of PSFs interacts with a scattering object to produce the individual receive-element signals (shown in scan converted format). Different PSFs were needed to account for the different relative positions of the elements in the receive aperture. Beamforming consists of combining the information from these individual elements into a single beamformed dataset (also shown scan converted) for subsequent envelope detection.

2.1 System model for receive element signals

In previous work[3,4], we have modeled the formation of RF data as a linear system, **H**, acting on a vector, **f**, representing the scattering profile of the object. In principle, **f** is a continuously defined function of 2 or (more appropriately) 3 dimensions. However, since the system that acts on it is inherently band limited, it is well approximated for our purposes by a discrete set of sample points. We restrict attention to the focal zone of the transmitted pulse, where the linear system can be efficiently implemented as a convolution with the pulse profile, but we note that the approach could be extended to more complicated linear system models. The resulting product of the system matrix with the object vector is corrupted by noise, **n**, to form the RF data vector, **g**.

We conceive of a similar process for generating the signal for each receive element in an aperture as shown in Figure 1. Let e be the index of the receive element (e = 1, ..., E), then a linear system model for the received signal of this element is given by

$$\mathbf{g}_e = \mathbf{H}_e\mathbf{f} + \mathbf{n}_e \qquad (1)$$

(note that in this work, boldface variables represent matrix and vector quantities). We see from Equation 1 that each receive element has its own system matrix, $\mathbf{H}_e$, and its own (independent) vector of acquisition noise, $\mathbf{n}_e$, but the object is common to all receiver elements.

We can assemble the linear systems specified in Equation 1 into a single system equation describing all elements simultaneously using block-matrix equations

$$\mathbf{g}_{\mathrm{RE}} = \begin{bmatrix} \mathbf{g}_1 \\ \mathbf{g}_2 \\ \vdots \\ \mathbf{g}_E \end{bmatrix} = \begin{bmatrix} \mathbf{H}_1 \\ \mathbf{H}_2 \\ \vdots \\ \mathbf{H}_E \end{bmatrix} \mathbf{f} + \begin{bmatrix} \mathbf{n}_1 \\ \mathbf{n}_2 \\ \vdots \\ \mathbf{n}_E \end{bmatrix} = \mathbf{H}\mathbf{f} + \mathbf{n} . \tag{2}$$

It is important for practical reasons to be aware of the size of the system, since it will limit what sorts of operations can reasonably be used in later steps. The number of elements in each $\mathbf{g}_e$ is the number of scan lines times the number of samples per scan line, and therefore the number of elements in $\mathbf{g}_{\mathrm{RE}}$ is that number times the number of elements. For the system we use in the simulation experiments described below, there are 128 scan lines, 256 samples per scan line (concentrated in the focal zone), and 92 receive elements for a total vector dimension of 3,145,728 in $\mathbf{g}_{\mathrm{RE}}$.

The role of beamforming is to compress the various element signals into a single RF signal, $\mathbf{g}_{\mathrm{BF}}$. If we consider a linear beamformer, we can write this as another linear transform

$$\mathbf{g}_{\mathrm{BF}} = \mathbf{B}\mathbf{g}_{\mathrm{RE}} . \tag{3}$$

We consider different approaches to defining $\mathbf{B}$ below in Section 2.4 after describing a set of tasks and the ideal observer in more detail.

2.2 Tasks for evaluating beamforming performance

We have developed a panel of simulation tasks for evaluating observer performance in detecting and discriminating various features of interest related to detection and diagnosis of breast cancer by ultrasound[10-12]. The five tasks were selected after consultation with a practicing mammographer who routinely uses ultrasound as an adjunct to X-ray mammography. These are simple classification tasks with two possible classes corresponding to our notions of benign and malignant.

Each task defines the variance profile of the object in the benign and malignant classes. The object vector is defined as a multivariate Gaussian random variable with each element being independent from all others, and with variance specified by the variance profile of the task and the class. For a given task, each object class is defined stochastically by a zero-mean multivariate Gaussian distribution. The use of zero-mean random variables for the object reflects the fact that we are not considering specular reflections. Thus the statistical differences between classes are entirely contained in the variance of the object. Let us denote objects from the benign class by $\mathbf{f}^-$ and those from the malignant class by $\mathbf{f}^+$. Then we can describe the distributions for each class as

$$\begin{aligned} \text{Benign: } \mathbf{f}^- &\sim \mathrm{MVN}\left(\mathbf{0}, \sigma_{\mathrm{obj}}^2 \left(\mathbf{I} + \mathbf{S}_0\right)\right) \\ \text{Malignant: } \mathbf{f}^+ &\sim \mathrm{MVN}\left(\mathbf{0}, \sigma_{\mathrm{obj}}^2 \left(\mathbf{I} + \mathbf{S}_1\right)\right), \end{aligned} \tag{4}$$

where σ_{obj}^2 is the generic variance of the object, and the diagonal matrices $\mathbf{S}_0$ and $\mathbf{S}_1$ represent the deviation from white noise in each class.

Figure 2 shows variance profiles for the five tasks used in this work. For clarity, the difference between the malignant and benign variance profiles is also shown. Task 1 represents detection of a 3mm low-contrast hypoechoic region. Tasks 2-4 all involve discriminating features from the boundary of a suspicious region. This corresponds to the frequent use of ultrasound for differential diagnosis of breast lesions in adjunct examinations. Task 2 considers lesion eccentricity with increased eccentricity being a sign of malignancy. Task 3 considers a soft margin as opposed to a well circumscribed boundary. Here, a soft margin is indicative of malignancy. Task 4 considers the presence of spiculations in the border as a malignant feature as compared to a smooth border, which tends to indicate a benign lesion. Finally,

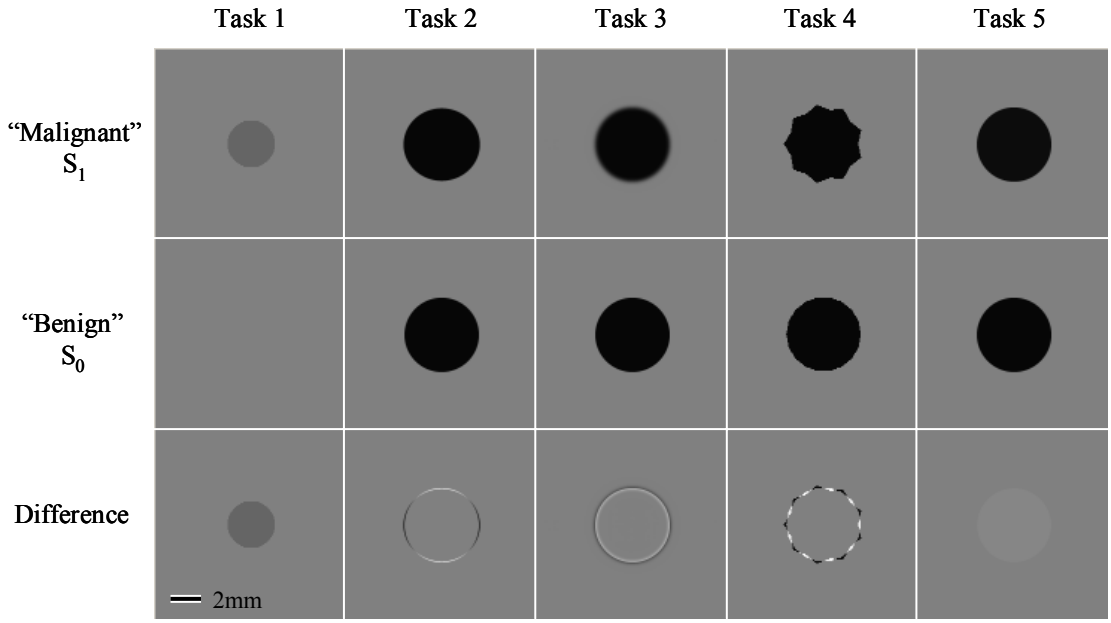

Figure 2. Visual tasks used to evaluate beamforming. The two variance profiles corresponding to the malignant (top) and benign (middle) classes for each task are shown along with difference between the two profiles.

Task 5 considers the presence of echogenic material in the lesion interior as a feature of malignant lesions as opposed to less echogenic interiors which might indicate a cyst or other benign finding.

2.3 The ideal observer

The ideal observer is defined as a statistically optimal discriminant function, and its decision variable for binary tasks such as the five we use is defined by the log-likelihood ratio of the data[5,7]. By considering many realizations of the decision variable we can build up figures of merit for task performance such as the area under the ROC curve or threshold contrast energy needed to achieve a specified task performance[13].

The ideal observer can be formulated at various stages of the imaging process. For example, we can consider an ideal observer that acts on the objects. Comparing the performance of an ideal observer before the imaging system acts has any effect allows us to see how much the imaging system degrades performance at later stages in processing. This loss of diagnostic information is captured by the efficiency metric which is comprised of a ratio of threshold contrast energies[13,14].

At the object stage, the ideal observer decision variable is given by

$$\lambda_{\text{obj}}(\mathbf{f}) = -\frac{1}{2\sigma_{\text{obj}}^2}\mathbf{f}^t\left(\left(\mathbf{I}+\mathbf{S}_1\right)^{-1}-\left(\mathbf{I}+\mathbf{S}_0\right)^{-1}\right)\mathbf{f}\,. \tag{5}$$

We can see that the ideal observer is a quadratic form in $\mathbf{f}$ that is weighted by the difference in inverse covariance matrices for the two classes. This general form is used throughout the imaging process. In order to obtain the ideal observer decision variable for receive element data, we must have an expression for the covariance matrix in both classes. Let $\mathbf{\Sigma}_{\text{RE},i}$ be the covariance matrix in class i ($i = 0,1$), then

$$\mathbf{\Sigma}_{\text{RE,i}} = \sigma_{\text{obj}}^2\mathbf{H}\left(\mathbf{I}+\mathbf{S}_i\right)\mathbf{H}^T+\sigma_n^2\mathbf{I}\,. \tag{6}$$

The resulting ideal observer decision variable for receive element data is then given by

$$\lambda_{\text{RE}}(\mathbf{g}) = -\frac{1}{2}\mathbf{g}^t\left(\mathbf{\Sigma}_{\text{RE},1}^{-1}-\mathbf{\Sigma}_{\text{RE},0}^{-1}\right)\mathbf{g}\,. \tag{7}$$

As described above, the decision variable is difficult to evaluate in this case because of the enormous size of the relevant covariance matrices. We discuss practical and theoretical implications of Equation 7 in the next section. For beam-

formed RF data, the relevant covariance matrices require propagating the variability in the receive element data through the beamforming matrix **B**, in Equation 3. In this case we obtain,

$$\mathbf{\Sigma}_{\mathrm{BF},i} = \mathbf{B}\mathbf{\Sigma}_{\mathrm{RE},i}\mathbf{B}^T = \sigma_{\mathrm{obj}}^2\mathbf{B}\mathbf{H}\left(\mathbf{I}+\mathbf{S}_i\right)\mathbf{H}^T\mathbf{B} + \sigma_n^2\mathbf{B}\mathbf{B}^T . \tag{8}$$

The resulting expression for the ideal observer decision variable is given by

$$\lambda_{\mathrm{BF}}\left(\mathbf{g}\right) = -\frac{1}{2}\mathbf{g}^t\left(\mathbf{\Sigma}_{\mathrm{BF},1}^{-1} - \mathbf{\Sigma}_{\mathrm{BF},0}^{-1}\right)\mathbf{g} . \tag{9}$$

Even though beamforming reduces the size of the covariance matrices considerably, they are still large enough (32,768 by 32,768 in this work) to be practically impossible. However, when **BH** is effectively a convolution, and noise in the beamformed data is white, we have developed a power-series approach to inverting the class covariance matrices that is computationally tractable.

2.4 Beamforming and the ideal observer

To begin our analysis of the ideal observer, we ask the question: should beamforming of receive element data be done at all? Equation 7, which gives the ideal observer decision variable for the receive element data, does not appear to have any obvious compression to a beamformed signal. So it might be the case that we lose information with any beamforming operation. To answer this question, we consider an argument based on the rank of the covariance component due to the object.

Equation 6 shows that the covariance matrix in each class is composed of a component due to the within-class variability of the object, and a second component due to the variability of the acquisition noise. Since the acquisition-noise component is full rank (for $\sigma_n > 0$), the whole covariance is guaranteed to be full rank, which is necessary for the existence inverse covariance matrices used to obtain the ideal observer decision variable. However, the covariance matrix due to the object is low-rank since **H** is a highly rectangular matrix with many more rows than columns (3,145,728 versus 32,768 in this work). Therefore, object variability in the receive-element data can be represented with a much lower dimensioned vector. This provides a theoretical justification for beamforming, since we can think of the operation as an attempt to transform receive element data to this lower dimensional space without loss of information.

The argument above implies that beamforming should be based on a subspace that avoids the null space of the covariance component due to the object. However, it is not straight-forward to find a basis for this subspace given the large sizes of the matrices involved. Thus, different beamforming approaches can be thought of as different ways to approximate an optimal information-preserving transform.

In this context, the standard delay-and-sum (DS) beamformer can be thought of as assuming that the information across the different elements is completely redundant, and therefore simply summing across the different elements (with delay correction) is optimal. If we consider the 2D discrete Fourier transform of the scan-converted receive-element signal, $g_e[k,l]$, or the delay-and-sum beamformed radio-frequency signal, $g_{\mathrm{DS}}[k,l]$, we find them related by

$$g_{\mathrm{DS}}\left[k,l\right] = \sum_{e=1}^{E} e^{-i\phi_e k} g_e\left[k,l\right], \tag{10}$$

where ϕ_e is the phase shift due to delay correction. Equation 10 shows that the sum across elements in beamforming is weighted by a phase factor in the Fourier domain that accounts for delays in acquisition timing. A more general phase term can be determined by considering the DFT of pulse profiles as transfer functions of the receive element systems. Let $h_e[k,l]$ be the transfer function for $\mathbf{H}_e$ (i.e. the DFT of the PSF), then we can implement a matched filter in phase (MFP) as a beamformer,

$$g_{\mathrm{MFP}}\left[k,l\right] = \sum_{e=1}^{E} \frac{\bar{h}_e\left[k,l\right]}{\left|h_e\left[k,l\right]\right|} g_e\left[k,l\right]. \tag{11}$$

This approach will correct for any interference in the sum due to the different pulse PSFs. This approach can also be arrived at by considering a Weiner filter applied to each element, and then summing across elements after normalizing for noise power at each frequency in every element. These two beamforming approaches are compared in the simulation studies

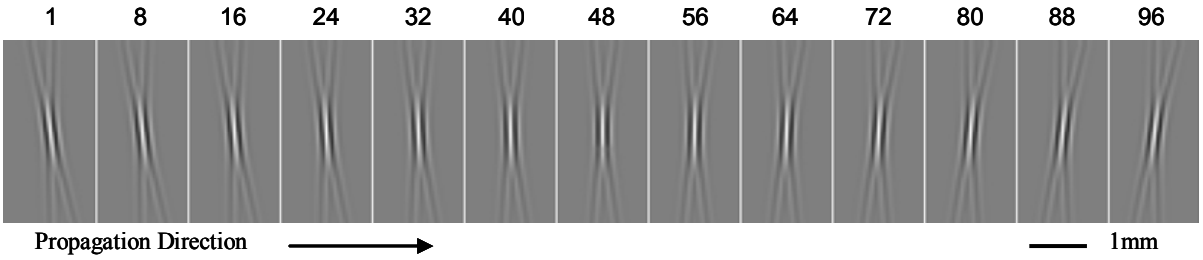

Figure 3. Receive element pulse profiles. The panel shows various receive element pulse PSFs. The pulse profile rotates with the receive element because of the relative position of each element in the receive aperture.

3. METHODS

3.1 System model using Field II

Figure 3 shows a more detailed view of the pulses profiles used in this work. These were generated using the Field II code developed by J.A. Jensen[8,9]. Parameters were set to model the Siemens Antares system with a VF10-5 linear array transducer. We used a 5MHz carrier frequency sampled at 40MHz; element pitch was set to 0.198mm with kerf of 5%; focus was set at 40mm depth; the transmit and receive aperture consisted of 96 elements (19 mm) scanned electronically over 192 elements. Echo SNR (peak power to noise) of the individual elements ranged between 6.6 and 7.2dB. After beamforming, echo SNR was approximately 45.4dB.

3.2 Monte-Carlo simulations

The receive-element PSFs were used in a simulation experiment where the two beamforming approaches in Equations 10 and 11 were compared. In both cases, the individual element PSFs were combined into a single beamformed PSF, and then the ideal observer approach we developed previously was applied to determine performance. The approach uses Monte-Carlo studies to develop a look-up table (LUT) for each task that plots performance as a function of the contrast energy difference between two object classes. This LUT is used to determine the threshold contrast needed to achieve a targeted performance. Performance is then given in terms of a detection or discrimination efficiency, the ratio of threshold contrast needed in the object domain – based on the decision variable specified in Equation 5 – compared to that in the beamformed RF domain – based on the decision variable in Equation 9.

In these simulations, we used proportion correct in a 2-alternative forced-choice paradigm as the measure, which is equivalent to area under an ROC curve. The targeted level of performance was 80% correct. In each task, 4 to 8 different contrast energies were evaluated. Interpolation between points in the LUT was done by linear interpolation in the detectability domain[3,4]. At each contrast evaluated in each task, 4,000 Monte-Carlo samples were generated from the malignant and benign classes respectively, and used to assess proportion correct.

4. RESULTS AND DISCUSSION

4.1 Differences in beamformed PSFs

Figure 4 compares the DS and MFP pulse PSFs. Spatially, the two pulses appear visually to be quite similar, with perhaps a slight improvement in lateral focusing in the MFP pulse. Images of pulse power in the 2D-FFT domain show a triangular region of the spatial frequency domain about the axial (horizontal) line that is transferred by the pulse. Again, it is difficult to clearly see any substantial differences between the two pulses. However, the image of the difference in pulse power between the MFP and DS pulses shows that substantial differences occur in frequencies corresponding to the axial line of the pulse. This is likely due to imperfect alignment in delay correction, since integer shifts were used rather than more computationally intensive interpolations. There is also a slight increase in pulse power over the off-axis region of the pulse. This increase shows the effect of the MFP which allows the different receive-element pulses to sum without interference.

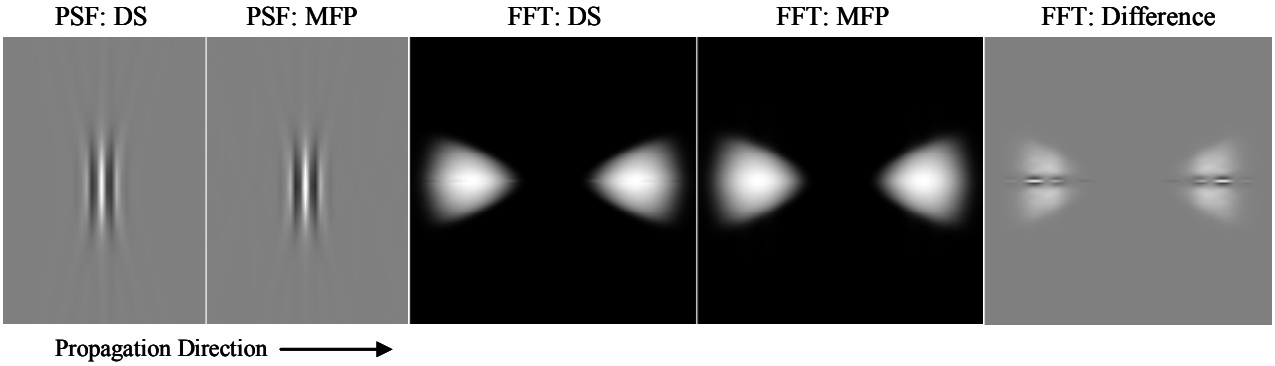

Figure 4. Beamformrd Pulse PSFs. The left two panes in the panel show pulse profiles of delay-and-sum (DS) and matched-filter in phase (MFP) beamformers. The next two panes show the pulse power in the 2D FFT domain. The difference in pulse power is shown on the right.

4.2 Performance differences between beamforming methods

Figure 5 is the main result of this work. The plot gives detection and discrimination efficiency in each of the five tasks evaluated for DS and MFP beamformers. Efficiency ranges in these tasks by approximately an order of magnitude, with a high point of 0.64 and a low point of less than 0.068. Highest efficiency is found in Tasks 1 and 5, the large-area tasks, with lower efficiency in Tasks 2-4, the boundary discrimination tasks. These results are consistent with previous studies using a Gabor function as for the beamformed pulse profile[3,4].

In all tasks except for Task 5, the MPF results in a substantial increase in efficiency. These efficiency improvements range from 35% in Task 1 to more than 100% in task 4. The results suggest that a substantial quantity of diagnostic information may be lost due to the inefficiency of the delay-and-sum beamformer.

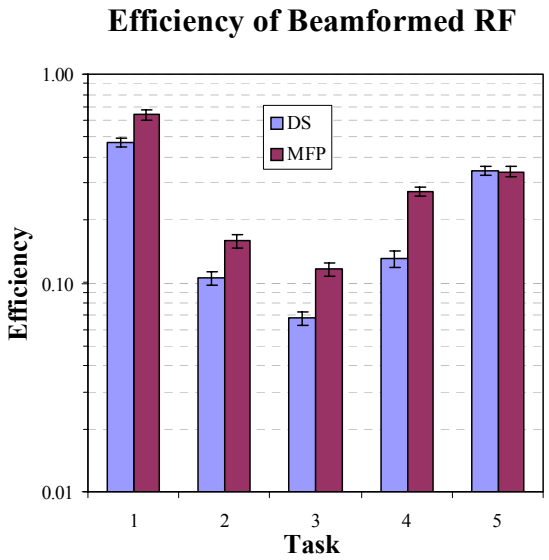

Figure 5. Task efficiency. Detection or discrimination efficiency is plotted on a log-scale as a function of the task number. Both delay and sum (DS) and matched-filter in phase (MFP) performance are plotted.

5. CONCLUSIONS

We have generalized the Ideal Observer approach from previous work to beamforming by extending a stochastic model of image formation to individual receive elements. This results in a different system model for each element as well as independent acquisition noise. Models of each receive-element system were assembled into a single large block-matrix system, and beamforming was implemented as a post-acquisition weighted sum across the individual elements. The receive element model can be used to specify the statistics of the element signals and to define an Ideal Observer decision variable.

In principle, the Ideal Observer decision variable could then be used to assess the element data directly through Monte-Carlo studies. However, since the ideal observer requires inverting the covariance matrix for the entire receive element dataset, it is practically impossible to implement without some insight to the covariance structure. We observe that since the covariance component due to the echo signals – as opposed to the acquisition noise – is relatively low rank, there is a lower dimensional signal that captures all the information about the object in the receive element dataset. This provides a rationale for beamforming from the Ideal Observer perspective. However, it is not clear what the appropriate beamforming transform should be.

Because the full decision variable is intractable, we have attempted to approximate the Ideal Observer by making a number of simplifying assumptions. We assume that the deviations of scattering variance in the object are small and that signal correlations among receive elements are negligible. With these assumptions we approximate the ideal observer

through a matched filter in the Fourier phase domain of 2D scan converted element data. This is followed by a summation across elements. We compare this approach to standard delay-and-sum beamforming using Monte-Carlo simulation in five tasks related to breast cancer imaging with ultrasound.

The evaluation of task performance shows a fairly substantial increase in detection and discrimination efficiency for most tasks. For example, low-contrast detection efficiency improves by approximately 35% while discrimination of a spiculated boundary improves by almost two-fold. One task, discrimination of increased echogenicity in the interior of a lesion, did not show any improvement with the phase domain matched filter beamformer. We speculate that the filter used is not well tuned to the lower scattering variance within the lesion, and therefore is unable to realize any improvements from beamforming. However, further analysis is needed to confirm the explanation.

ACKNOWLEDGMENTS

This work was supported in part by the NCI under award No. CA118294.

REFERENCES

1. A. Macovski, *Medical Imaging Systems* (Prentice-Hall, Englewood Cliffs, NJ), 1983.
2. B.A.J. Angelsen, *Ultrasonic Imaging*: Waves, Signals, and Signal Processing (Emantec AS, Trondheim, Norway) 2000.
3. C.K. Abbey, R.J. Zemp, J. Liu, K.K. Lindfors, and M.F. Insana, "Observer efficiency in discrimination tasks simulating malignant and benign breast lesions imaged with ultrasound," *IEEE Trans. Med. Imag. 25*(2): 198-209, 2006.
4. C.K. Abbey, R.J. Zemp, J. Liu, K.K. Lindfors, and M.F. Insana, "Observer Efficiency in Boundary Discrimination Tasks Related to Assessment of Breast Lesions with Ultrasound," *Proc. SPIE Med. Imag.* (*Y. Jiang and M.P. Eckstein Ed.s*), Vol. 6146, 2006.
5. A.D. Whalen, *Detection of Signals in Noise*, (Academic Press, San Diego, CA) 1971.
6. H.H. Barrett, C.K. Abbey, and E. Clarkson, "Objective assessment of image quality. III. ROC metrics, ideal observers, and likelihood-generating functions," *J Opt Soc Am A,* 15 (6):1520-35, 1998.
7. H. L. Van Trees, *Detection, Estimation, and Modulation Theory* (Wiley, New York, NY), Vol. I, 1968.
8. J.A. Jensen and N. B. Svendsen, "Calculation of pressure fields from arbitrarily shaped, apodized, and excited ultrasound transducers," *IEEE Trans. Ultrason., Ferroelec., Freq. Contr.*, 39:262-267, 1992.
9. J. A. Jensen. Field: A program for simulating ultrasound systems. *Med. Biol. Eng. Comp.*, 10th Nordic-Baltic Conference on Biomedical Imaging, Vol. 4, Supplement 1, Part 1:351–353, 1996.
10. *Breast Imaging Reporting and Data System Atlas*. Reston, VA: American College of Radiology, 2003.
11. L. W. Bassett and C. Kimme-Smith, "Breast sonography," *Am. J. Roentgenol.*, vol. 156, no. 3, pp. 449–455, 1991.
12. H. M. Zonderland, E. G. Coerkamp, J. Hermans, M. J. van de Vijver, and A. E. van Voorthuisen, "Diagnosis of breast cancer: Contribution of US as an adjunct to mammography," *Radiology*, vol. 213, no. 2, pp. 413–422, 1999.
13. D.M. Green and J.A. Swets, *Signal Detection Theory and Psychophysics*, Wiley, NY, 1966.
14. W.P. Tanner and T.G. Birdsall, "Definitions of d' and η as psychophysical measures," In: *Signal Detection and Recognition by Human Observers: Contemporary Readings* (J.A. Swets, ed.), Wiley, NY, 1964.
15. A.E. Burgess, "Comparison of receiver operating characteristic and forced choice observer performance measurement methods." *Med Phys*. vol. 22(5), pp. 643-55, 1995.